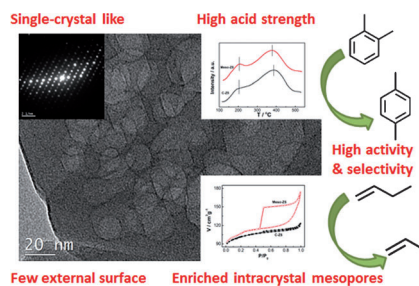


COMMUNICATIONS

Sowing the seeds: A sub-micron single-crystal-like ZSM-5 catalyst with enriched intracrystal mesopores is synthesized through a facile organic structure-directing agent-free and seed-induced route. The special crystal structure leads to significantly improved catalytic activity, well-preserved shape selectivity, and slow deactivation in the isomerization of *o*-xylene to *p*-xylene.



H. Zhang, K. Song, L. Wang, H. Zhang,
Y. Zhang, Y. Tang*



Organic Structure Directing Agent-Free and Seed-Induced Synthesis of Enriched Intracrystal Mesoporous ZSM-5 Zeolite for Shape-Selective Reaction



DOI: 10.1002/cctc.201300242

Organic Structure Directing Agent-Free and Seed-Induced Synthesis of Enriched Intracrystal Mesoporous ZSM-5 Zeolite for Shape-Selective Reaction

Hongbin Zhang, Kunshan Song, Lei Wang, Hongxia Zhang, Yahong Zhang, and Yi Tang*^[a]

Zeolites, a family of crystalline aluminosilicate materials, have been widely used as shape-selective catalysts, ion-exchange materials, and adsorbents for their well-defined micropores, large surface areas, high acidity, and high hydrothermal stability.^[1] Initially, low silica zeolites were synthesized without any organic structure directing agent (OSDA), for example A, X, Y, L, and mordenite zeolites. With the employment of OSDAs, mainly tetraalkylammonium ions, high silica zeolites were discovered, such as ZSM-5, Beta, ZSM-11, and ZSM-12. However, the introduction of OSDAs could lead to high cost, complex synthesis processes, large energy consumption for detemplating by calcination, and severe environmental issues. From 2009 to 2012, OSDA-free and seed-induced synthesis strategies were adopted to prepare various framework zeolites including ZSM-5,^[2] BEA,^[3] ZSM-34,^[4] RUB-13,^[5] and ZSM-12.^[6]

Traditional zeolite crystals with the sole micropores often suffer serious mass transfer problems leading to low utilization of active sites and poor catalytic activity.^[7] To overcome this problem, great effort has been put into the synthesis of wide-pore zeolites, nanosized zeolites, zeolite composites, and mesoporous zeolite crystals.^[7a,e-h] Among these materials, mesoporous zeolite has attracted increasing attention because it combines the advantages of both mesoporous materials and zeolite crystals. From 2006 to 2012, various strategies were proposed to synthesize mesoporous zeolites, such as the zeolitization of a mesoporous material, crystallization with micro- and mesoporous templates, assembly of nanosized zeolites, recrystallization, and demetalization.^[7] However, for an industrial evaluation, there are still some drawbacks for these strategies with respect to manufacturing costs, material characteristics, health and safety, and environmental considerations.^[7a,f,h,8]

Herein, a facile OSDA-free seed-induced route is proposed for fast synthesis of sub-micron sized ZSM-5 zeolite with enriched intracrystal mesopores (denoted as Meso-Z5), which was prepared typically by the simple addition of 200 nm silica-lite-1 seed (7 wt%) into a KF-containing starting gel with the molar ratio of $\text{SiO}_2/\text{Al}_2\text{O}_3/\text{Na}_2\text{O}/\text{KF}/\text{H}_2\text{O}$ 1:(0–0.025):0.15:

(0–0.9):50 and further hydrothermal crystallizing at 180 °C (see the Experimental Section). The introduction of seeds makes product crystallization very rapid (typically 2 h, Figure S1) and produces high yield (> 70%), even without OSDA, whereas the addition of KF and aging time are crucial to modulate the amount and size of mesopores and the crystallinity of the products. The combination of their abundant intracrystal mesopores and perfect micropore structure are proved to have notable catalytic activity and good shape selectivity for the isomerization of *o*-xylene. Such an approach for the fast and facile preparation of single-crystal-like zeolite with enriched intracrystal mesopores may bring new possibilities for developing novel structured zeolites and their scale-up production for industrial applications.

SEM and TEM images of a typical Meso-Z5 sample (synthesized with KF/Si molar ratio=0.6, aging time=6 h) are displayed in Figure 1. After crystallization for only 2 h, the product

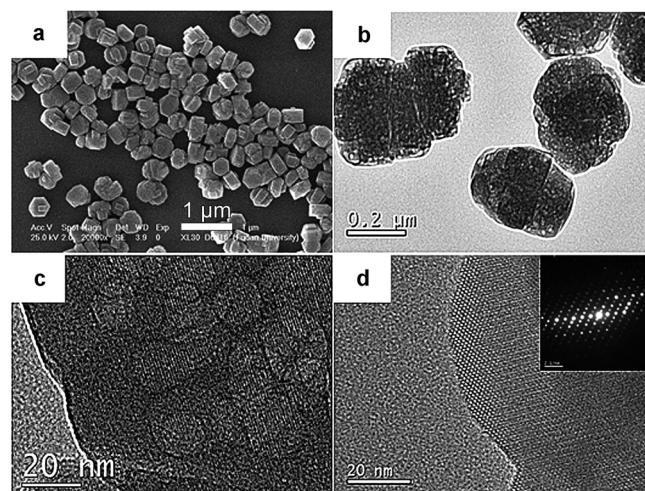


Figure 1. a) SEM, b,c) TEM, d) HRTEM, and selected area (electron) diffraction images (inset of part d) of Meso-Z5.

exhibits approximately 400 nm-sized irregular hexagonal morphologies with smooth external surfaces (Figure 1 a), whereas the TEM images show that all zeolite crystals are pervaded with enriched randomly oriented mesopores 10–40 nm in size (Figure 1 b and c). The TEM image at high magnification (Figure 1 c) further proves that each particle is similar to a single crystal with high crystallinity for the clear lattice fringes extending over the entire particle. Moreover, the high resolution TEM (HRTEM) image in Figure 1 d indicates the uniform micro-

[a] H. Zhang, K. Song, L. Wang, H. Zhang, Prof. Y. Zhang, Prof. Y. Tang
Department of Chemistry
Shanghai Key Laboratory of Molecular Catalysis and Innovative Materials
Laboratory of Advanced Materials
and Collaborative Innovation Center of Chemistry for Energy Materials
Fudan University
Shanghai 200433 (P.R. China)
Fax: (+86)21-65641740
E-mail: yitang@fudan.edu.cn

Supporting information for this article is available on the WWW under <http://dx.doi.org/10.1002/cctc.201300242>.

pore structure of the particle surface with the thickness of approximately 30–60 nm and the inset of the selected area (electron) diffraction image presents a light and clear diffraction pattern of the single-crystal ZSM-5 zeolite.

The unique features of Meso-Z5 can be described further by comparing it with commercial H-ZSM-5 (4 μm and rectangle shape, shown in Figure S2a, denoted as C-Z5). As shown in Figure 2a, the Meso-Z5 sample displays the pure XRD pattern of the MFI framework with very sharp diffraction peaks almost the same as those of C-Z5. The N_2 sorption isotherms of these two samples are presented in Figure 2b. The C-Z5 with larger single-crystal structure displays only a steep increase in the curve at very low relative pressure ($P/P_0 < 0.2$), almost without an adsorption hysteresis loop, corresponding to the typical nitrogen adsorption isotherm of microporous material. For the sample of Meso-Z5, however, in addition to the steep adsorption at low pressures, an additional type H4 hysteresis loop is present at $P/P_0 = 0.43$ –1, corresponding to the materials with the composited structure of both micropores and mesopores.^[9] Remarkably, a characteristic decrease is observed in the desorption branch at $P/P_0 \approx 0.43$ and the size of the hysteresis loop (i.e., the difference in adsorption volume between desorption and adsorption branches) is as large as almost $40 \text{ cm}^3 \text{ g}^{-1}$. As the TEM images in Figure 1b and c show that the sample contains abundant embedded mesopores amid the micropore framework structure, this special hysteresis loop can be ascribed to the tensile strength or cavitation effects induced by the pore networks of ink bottle-type, in which desorption from the pore body occurs suddenly after the neck is emptied.^[9,10] The hysteresis loop closure pressure at $P/P_0 = 0.43$ depends on the physical properties of the adsorbate N_2 at 77 K because the size of the pore neck of, in this case, the ZSM-5 micropore is far below that of the critical value for N_2 .^[9,10] Therefore, the adsorption data are used to calculate the pore size distribution by the Barrett–Joyner–Halenda method to avoid the misinterpretation of uniform mesopores of 4 nm.^[10] As shown in Figure 2c, Meso-Z5 has a wide mesopore distribution between 10 and 40 nm based on intracrystal mesopores, which is in good agreement with the TEM image in Figure 1c. The textural data (Table 1) indicate that, although Meso-Z5 has almost the same Langmuir surface area ($S_L = 480 \text{ m}^2 \text{ g}^{-1}$) and microporous volume ($V_{\text{micro}} = 0.11 \text{ cm}^3 \text{ g}^{-1}$) as those of C-Z5 ($S_L = 460 \text{ m}^2 \text{ g}^{-1}$ and $V_{\text{micro}} = 0.13 \text{ cm}^3 \text{ g}^{-1}$), the former has a much larger mesoporous volume ($V_{\text{meso}} = 0.20 \text{ cm}^3 \text{ g}^{-1}$) than the latter ($V_{\text{meso}} = 0.05 \text{ cm}^3 \text{ g}^{-1}$) with a slightly larger external

Sample	Si/Al ^[a]	S_L [$\text{m}^2 \text{ g}^{-1}$]	S_{ext} ^[b] [$\text{m}^2 \text{ g}^{-1}$]	V_{micro} ^[b] [$\text{cm}^3 \text{ g}^{-1}$]	V_{meso} ^[c] [$\text{cm}^3 \text{ g}^{-1}$]
C-Z5	36	460	52	0.13	0.05
Meso-Z5	34	481	87	0.11	0.20

[a] Molar ratio determined by using X-ray fluorescence spectroscopy;
 [b] Obtained by using the t -plot method (S_{ext} = external surface area);
 [c] Obtained by using the Barrett–Joyner–Halenda method with the adsorption branch.

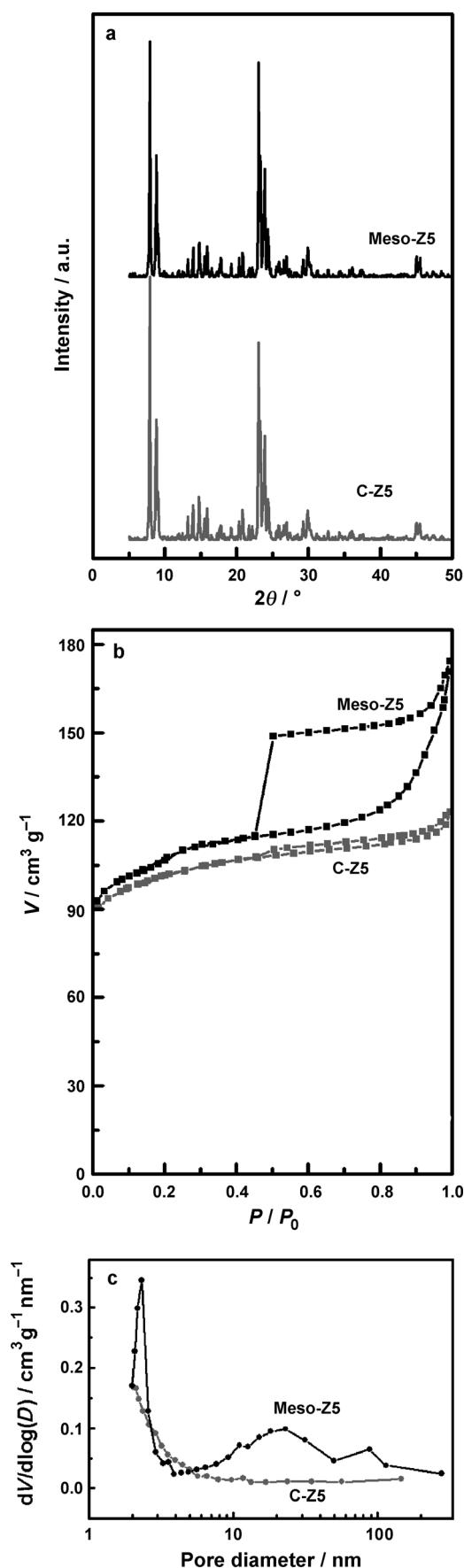


Figure 2. a) XRD patterns, b) N_2 isotherms, and c) pore size distributions for C-Z5 and Meso-Z5.

surface area. The presence of mesopores in Meso-Z5 would effectively interconnect the micropores to offer additional diffusional paths for catalysis.

The acidic Meso-Z5 was obtained by ion-exchange repeated three times with NH_4NO_3 aqueous solution at 90°C for 3 h and then calcined at 550°C for 5 h. The acidities of C-Z5 and Meso-Z5 were characterized by NH_3 temperature-programmed desorption (NH_3 -TPD; Figure S3). Their similar peak areas indicate the similar number of total acid sites in these two samples, which is consistent with their similar Si/Al ratio in Table 1. Moreover, the TPD curves of these samples have almost the same profiles with two desorption peaks with maxima of approximately 220 and 390°C , indicating the similar strength and ratio of weak and strong acid amounts. These results suggest that the strength and amount of the Brønsted sites are well-maintained during the introduction of abundant mesopores.

Meso-Z5 and C-Z5 were applied to *o*-xylene isomerization, which is a model reaction to assess the shape selectivity of microporous materials and a major industrial application of zeolites for the most desired *p*-xylene.^[11] All catalytic results (conversion, selectivity, and stability) in Figure 3 were acquired on a fixed-bed reactor equipped with an online GC for product analysis. The reaction temperature was 673 K , the weight hourly space velocity (WHSV) 5.0 h^{-1} , and the pressure 1 atm . The product distribution analysis indicated that the main products were the xylenes of three isomers and almost no disproportionation reaction occurred. As shown in Figure 3a, the *o*-xylene conversion on Meso-Z5 (about 60%) was far higher than that on C-Z5 (about 30%) during the whole reaction run, owing probably to its reduced diffusion limitations by the introduction of extensive intracrystal mesopores (Figures 1b and

2c and Table 1). Although with super activity on Meso-Z5, its *p*-xylene selectivity ($\approx 35.5\%$) was only slightly lower than that on C-Z5 ($\approx 40.0\%$), as shown in Figure 3b. The phenomena could be explained by the special structure of Meso-Z5. As the abundant mesopores were occluded in the microporous matrix by a well-crystallized microspore layer (thickness of $\approx 30\text{--}60\text{ nm}$, Figures 1c,d and 2a,b), the amount of acid sites on the external surface should have been similar to that of C-Z5. Therefore, the *para*-selectivity of the Meso-Z5 was well-maintained for the favor of monomolecular reaction within the microporous network, whereas the slight decrease of the *para*-selectivity of Meso-Z5 compared with that of C-Z5 could be attributed to the shortening of the shape-selective micropore length. Overall, the hierarchical ZSM-5 displayed an approximately twofold increase in *p*-xylene yield compared to the pure micropore C-Z5 (21% for Meso-Z5 vs. 12% for C-Z5 in Figure 3c). Moreover, Meso-Z5 represents a distinctive advantage in the stability on *o*-xylene isomerization for its slower deactivation than C-Z5 shown in Figure 3d. This may result from 1) the few external surface acid sites, 2) the well-interconnecting micropore channels by abundant embedded mesopores, and 3) the corresponding large tolerability of Meso-Z5 to coke.

A sub-micrometer sized HZSM-5 sample (denoted as SM-Z5) without intracrystal mesopores but with similar particle size, shape, and acid amount (Si/Al=32) to Meso-Z5 was synthesized to more clearly distinguish the effects of particle sizes and mesopore properties on the *o*-xylene isomerization reaction, as shown in Figure S4. This SM-Z5 sample displayed an improved catalytic activity ($\approx 46\%$) compared with C-Z5 ($\approx 30\%$) that was, however, lower than that of Meso-Z5 ($\approx 60\%$) and it showed a similar selectivity ($\approx 34\%$) to that of Meso-Z5 (35%). Therefore, the introduction of intracrystal mesopores did provoke the observed effect of increased conversion in *o*-xylene conversion in addition to the role of particle size. For further understanding of this reaction, the adsorption and diffusion of *o*-xylene on the three samples were also tested to investigate the interaction between the *o*-xylene molecules and HZSM-5 zeolites with different morphologies by a gravimetric analyzer. As shown in Figure S5, Meso-Z5 displayed not only the fastest adsorption rate but the highest adsorption capacity, which probably results from the shortened diffusion length and a subtle interplay of increased sorbate-sorbate interactions and/or highly energetically heterogeneous surfaces caused by the introduction of abundant

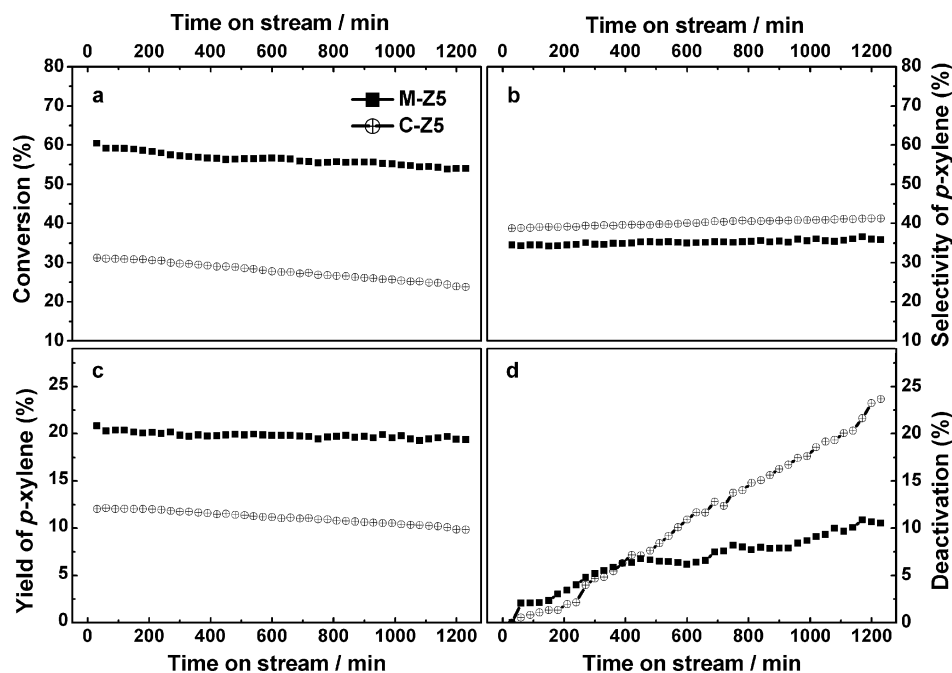


Figure 3. a) Conversion of *o*-xylene, b) selectivity to *p*-xylene, c) yield of *p*-xylene, and d) deactivation of catalysts over C-Z5 and Meso-Z5. The deactivation is defined as $(X_0 - X_t)/X_0$, in which X_0 is the initial *o*-xylene conversion and X_t is the *o*-xylene conversion at time t .

mesopores.^[12] On the other hand, a non-aqueous potentiometric titration measurement with *tert*-butylamine (the solvent diameter, 0.68 nm, was larger than the micropore size of zeolite ZSM-5, ≈ 0.54 nm) in Figure S6 showed a similar number of accessible acid sites on the external surface for the C-Z5, SM-Z5, and Meso-Z5.^[8] These experimental facts demonstrated that 1) the Meso-Z5 sample had abundant mesopores to reduce diffusion limitations for increasing the conversion, 2) the special intracrystal mesoporous structure (the mesopores were connected to the gas phase by shape-selective MFI-type micropores) was beneficial in maintaining the shape selectivity to *p*-xylene, and 3) the few external surface acid sites benefiting from this special structure would lead to few undesired secondary reactions of the *p*-xylene product.

Further investigation reveals that the addition of KF and the duration of aging time are two crucial factors for the modulation of the introduction of mesopores and the crystallinity of samples. The XRD patterns for the samples with KF/Si = 0–0.90 (Figure S7) all display characteristic patterns of the typical MFI structure. The N₂ isotherms and pore size distributions of the samples are presented in Figures S8 and S9. No hysteresis loop in N₂ sorption isotherm is observed at KF/Si = 0, indicating that the special intracrystal mesopore structure cannot be obtained in the absence of KF. The hysteresis loop appears with the addition of KF. Interestingly, the samples synthesized with different KF content have different hysteresis loop sizes; the amount and size of the mesopores in Meso-Z5 increase with respect to KF/Si molar ratio in the order of $0.60 > 0.30 > 0.15$, as according to the TEM images in Figure S10. This sequence is parallel to the size of the hysteresis loop. However, at KF/Si = 0.9, both surface area and hysteresis loop size decrease, implying partial damage of the framework owing to the structure-breaking effect of K⁺.^[13] To prepare Meso-Z5 with well-preserved microporous structure, the effect of prolonging the aging time from 1.5 to 12 h is also investigated. The XRD patterns in Figure S11 indicate that all products are of typical MFI structure and longer aging time results in higher crystallinity. According to the N₂ isotherms and pore size distributions in Figures S12 and S13, the suitable aging time is 6 h if the larger amount of mesopores and the higher crystallinity are kept synchronous.

The catalytic study has also been extended to four Meso-Z5 samples with different mesopore contents and sizes (Figure S10) to investigate their relationship to catalytic properties in *o*-xylene isomerization. Considering the higher Si/Al ratio (≈ 44) of these Meso-Z5 samples, the reaction temperature was increased to 723 K and the WHSV decreased to 2.5 h⁻¹ to investigate the catalytic differences. As shown in Figure S14, the *p*-xylene yield curve displayed a volcano curve in which a better catalytic result was observed for the samples of KF/Si = 0.3–0.6 with higher conversion ($\approx 66\%$) and well-maintained *p*-xylene selectivity ($\approx 33\%$). On increasing the KF/Si ratio to 0.9, the amount of mesopores decreased a lot, which led to lower conversion ($\approx 49\%$) and similar selectivity ($\approx 34\%$). At KF/Si = 0.15, as more nano-particle stacked structures result in a large external surface, the selectivity ($\approx 30\%$) decreased. The slightly lower conversion ($\approx 58\%$) owed proba-

bly to the decreased size of mesopores or the small reduction in their quantity.

In summary, a facile and fast synthesis of KF-aided OSDA-free, seed-induced hydrothermal process is proposed for the environmentally friendly and low-cost production of high-quality single-crystal ZSM-5 zeolite with enriched intracrystal mesopores (Meso-Z5). This Meso-Z5 displays catalytic performances with a twofold *p*-xylene yield compared to C-Z5 in *o*-xylene isomerization, owing to the greatly improved activity and well-preserved selectivity. The quantity and size of mesopores and the crystallinity can be controlled easily by changing the addition of KF and the duration of aging time. Notably, this method can be easily extended to synthesize mesoporous ZSM-5 zeolite with high Si/Al molar ratio (Si/Al > 100, denoted as Meso-EA-Z5) by simply adding a small amount of cheap ethylamine (ethylamine/Si molar ratio = 0.1) to the system. The preliminary study indicates that the special intracrystal mesopore structure plays an important role in butene cracking reactions to greatly enhance propene selectivity and well-preserve butene conversion (see Table S1 and Figure S15).

Experimental Section

Syntheses: The seeds with the crystal size of 200 nm were presynthesized by using a clear solution method.^[14] Typically, for the synthesis of intracrystal mesoporous single-crystal-like ZSM-5 zeolite (Meso-Z5), a starting aluminosilicate mixture with a molar ratio of SiO₂/Al₂O₃/Na₂O/KF/H₂O 1:(0–0.025):0.15:(0–0.9):50 was prepared by using Al₂(SO₄)₃·18H₂O as the alumina source and 40% colloidal silica as the silica source. The preprepared silicalite-1 seed solution was then added under stirring. The addition quantity of seed typically equaled 7.0 wt% of total SiO₂ weight in the starting gel. Then, the mixture was stirred at ambient temperature for 1.5–12 h and treated hydrothermally at 180 °C for 0.5–5 h. The obtained zeolites were separated by filtration, then washed with deionized water, dried at 120 °C for 6 h, and finally calcined under static air at 550 °C for 5 h. The intracrystal mesoporous single-crystal-like ZSM-5 zeolite with high Si/Al molar ratio (Meso-EA-Z5) was prepared under the same conditions as Meso-Z5, except that a small amount of ethylamine (ethylamine/Si molar ratio = 0.1) was added.

Reference samples: Two commercial H-ZSM-5 samples with low Si/Al molar ratio of 36 (denoted as C-Z5) and high Si/Al molar ratio of 145 (denoted as C-HS-Z5) (both from Nankai Catalyst Company) were employed as references to investigate the advantages of Meso-Z5 and Meso-EA-Z5. The SEM images in Figure S2 clearly show the size and crystal morphology of the C-Z5 (4 μ m, rectangular) and C-HS-Z5 samples (3 μ m, coffin-shaped). The sub-micrometer sized HZSM-5 sample (denoted as SM-Z5) was synthesized by a seed-induced method according to our previous work.^[2b] This sample did not contain mesopores but had a similar size, shape, and number of acid sites (Si/Al = 32) to Meso-Z5 (see Figure S4, including SEM, XRD, N₂ sorption isotherm, and catalytic performance results).

Acknowledgements

This work is supported by the 973 programme (2013CB934101, 2009CB623506, and 2009CB930400) and STCMS (09DZ2271500 and 11JC1400400).

Keywords: crystal growth · heterogeneous catalysis · isomerization · mesoporous materials · zeolites

- [1] a) A. Corma, *Chem. Rev.* **1995**, *95*, 559–614; b) A. Corma, *Chem. Rev.* **1997**, *97*, 2373–2419; c) C. S. Cundy, P. A. Cox, *Chem. Rev.* **2003**, *103*, 663–701; d) M. E. Davis, *Nature* **2002**, *417*, 813–821.
- [2] a) G. Majano, A. Darwiche, S. Mintova, V. Valtchev, *Ind. Eng. Chem. Res.* **2009**, *48*, 7084–7091; b) N. Ren, Z. J. Yang, X. C. Lv, J. Shi, Y. H. Zhang, Y. Tang, *Microporous Mesoporous Mater.* **2010**, *131*, 103–114.
- [3] a) B. Xie, H. Y. Zhang, C. G. Yang, S. Y. Liu, L. M. Ren, L. Zhang, X. J. Meng, B. Yilmaz, U. Muller, F. S. Xiao, *Chem. Commun.* **2011**, *47*, 3945–3947; b) Y. Kamimura, W. Chaikittisilp, K. Itabashi, A. Shimojima, T. Okubo, *Chem. Asian J.* **2010**, *5*, 2182–2191; c) G. Majano, L. Delmotte, V. Valtchev, S. Mintova, *Chem. Mater.* **2009**, *21*, 4184–4191.
- [4] C. G. Yang, L. M. Ren, H. Y. Zhang, L. F. Zhu, L. Wang, X. J. Meng, F. S. Xiao, *J. Mater. Chem.* **2012**, *22*, 12238–12245.
- [5] T. Yokoi, M. Yoshioka, H. Ima, T. Tatsumi, *Angew. Chem.* **2009**, *121*, 10068–10071; *Angew. Chem. Int. Ed.* **2009**, *48*, 9884–9887.
- [6] K. Iyoki, Y. Kamimura, K. Itabashi, A. Shimojima, T. Okubo, *Chem. Lett.* **2010**, *39*, 730–731.
- [7] a) J. Pérez-Ramírez, C. H. Christensen, K. Egeblad, C. H. Christensen, J. C. Groen, *Chem. Soc. Rev.* **2008**, *37*, 2530–2542; b) D. Verboekend, J. Pérez-Ramírez, *Catal. Sci. Technol.* **2011**, *1*, 879–890; c) X. J. Meng, F. Nawaz, F. S. Xiao, *Nano Today* **2009**, *4*, 292–301; d) K. Egeblad, C. H. Christensen, M. Kustova, C. H. Christensen, *Chem. Mater.* **2008**, *20*, 946–960; e) J. Čejka, S. Mintova, *Catal. Rev. Sci. Eng.* **2007**, *49*, 457–509; f) R. Chal, C. Gerardin, M. Bulut, S. van Donk, *ChemCatChem* **2011**, *3*, 67–81; g) Y. S. Tao, H. Kanoh, L. Abrams, K. Kaneko, *Chem. Rev.* **2006**, *106*, 896–910; h) L. H. Chen, X. Y. Li, J. C. Rooke, Y. H. Zhang, X. Y. Yang, Y. Tang, F. S. Xiao, B. L. Su, *J. Mater. Chem.* **2012**, *22*, 17381–17403.
- [8] H. Zhang, Y. Ma, K. Song, Y. Zhang, Y. Tang, *J. Catal.* **2013**, *302*, 115–125.
- [9] M. Thommes, *Chem. Ing. Tech.* **2010**, *82*, 1059–1073.
- [10] J. C. Groen, J. Pérez-Ramírez, *Appl. Catal. A* **2004**, *268*, 121–125.
- [11] a) C. Fernandez, I. Stan, J. P. Gilson, K. Thomas, A. Vicente, A. Bonilla, J. Pérez-Ramírez, *Chem. Eur. J.* **2010**, *16*, 6224–6233; b) M. Guisnet, N. S. Gnep, S. Morin, *Microporous Mesoporous Mater.* **2000**, *35*, 47–59; c) W. Vermeiren, J. P. Gilson, *Top. Catal.* **2009**, *52*, 1131–1161.
- [12] a) V. R. Choudhary, V. S. Nayak, T. V. Choudhary, *Ind. Eng. Chem. Res.* **1997**, *36*, 1812–1818; b) M. O. Daramola, A. J. Burger, M. Pera-Titus, A. Giroir-Fendler, S. Miachon, J. A. Dalmon, L. Lorenzen, *Asia Pac. J. Chem. Eng.* **2010**, *5*, 815–837; c) G. Muller, T. Narbeshuber, G. Mirth, J. A. Lercher, *J. Phys. Chem.* **1994**, *98*, 7436–7439.
- [13] J. A. Ke, I. Wang, *Mater. Chem. Phys.* **2001**, *68*, 157–165.
- [14] A. E. Persson, B. J. Schoeman, J. Sterte, J. E. Ottesstedt, *Zeolites* **1994**, *14*, 557–567.

Received: March 29, 2013

Revised: May 23, 2013

Published online on ■ ■ ■, 0000